Density, compressibility and phase equilibrium of high pressure-high temperature reservoir fluids up to 473 K and 140 MPa

Regueira Muñiz, Teresa; Glykioti, Maria-Lito; Kottaki, Nomiki; Stenby, Erling Halfdan; Yan, Wei

Published in:
Journal of Supercritical Fluids

Link to article, DOI:
10.1016/j.supflu.2020.104781

Publication date:
2020

Document Version
Peer reviewed version

Density, compressibility and phase equilibrium of high pressure-high temperature reservoir fluids up to 473 K and 140 MPa

Teresa Regueira, Maria-Lito Glykioti, Nomiki Kottaki, Erling H. Stenby, Wei Yan*
Center for Energy Resources Engineering (CERE), Department of Chemistry, Technical University of Denmark, DK-2800 Kgs. Lyngby, Denmark
*Corresponding author: E-mail: weya@kemi.dtu.dk; Tel.:+45 45252379

Abstract

Experimental measurement of volumetric and phase equilibrium properties of two high pressure - high temperature reservoir fluids was performed in this work. One fluid is volatile oil and the other is gas condensate. The density, isothermal compressibility, saturation pressure, and liquid fraction below the saturation pressure were determined in the temperature range up to 473.15 K by using a high pressure vibrating tube densitometer and a PVT cell. The obtained data were modelled by using equations of state including Soave-Redlich-Kwong (SRK), Peng-Robinson (PR), volume translated SRK (SRK-VT), volume translated PR (PR-VT) and Perturbed-Chain Statistical Association Fluid Theory (PC-SAFT). Among these models, the performance in saturation pressure prediction is system-dependent and it is hard to generalize the observation. PC-SAFT models volumetric properties satisfactorily. Regarding density calculation, it performs similarly to SRK-VT and PR-VT for the two fluids investigated here. Concerning isothermal compressibility, PC-SAFT is slightly better.

Keywords: density, compressibility, phase equilibrium, high pressure – high temperature, reservoir fluid

1. Introduction

The global increase in energy consumption puts a higher demand for energy from different sources including gas and oil. This has led to two clear changes in the oil and gas industry: development of unconventional resources, such as shale production in the US, and exploitation of oil and gas in more challenging environments, such as on-shore or offshore deep reservoirs usually at high pressures and high temperatures. Many of the high-pressure reservoirs related

to the second change can be classified as high pressure - high temperature (HPHT) reservoirs, which, in the oil and gas industry, often refer to reservoirs with pressures higher than 69 MPa and temperatures higher than 422.15 K. These limits are somewhat arbitrary and HPHT generally indicates more extreme pressure and temperature conditions where we have less experience with and a much wider temperature and pressure range that the production needs to cover. Development of those reservoirs present numerous challenges in terms of safety, testing, seals, and materials [1]. A central issue is how to realize a cheaper, safer and more efficient development of these reservoirs.

The importance of fundamental thermodynamic properties for relevant HPHT systems can never be overestimated. The availability of thermodynamic properties of the reservoir fluids under these extreme conditions is low and there is only a limited experience in the industry in performing the standard PVT studies at very high pressure and temperature conditions [2]. The volumetric and phase equilibrium properties are necessary for the estimation of oil and gas resources and the description of the dynamic production process which involves single-phase expansion, phase transition and vapour-liquid equilibrium in the two-phase region. Density and compressibility play a crucial role in production forecast of the pressure depletion process [2, 3], as compressibility is a driving force in the primary recovery. Regarding gas condensates, once the reservoir pressure decreases below the saturation pressure, valuable liquid hydrocarbons can drop out and tend to stay in the reservoir [4]. The maximum liquid fraction below the saturation pressure for the gas condensates indicates the richness of the gas condensate [5]. It is desirable to avoid large drop-out since the condensate drop-out near the wellbore can decrease the gas relative permeability dramatically and thus the well productivity, which is known as condensate blocking [4, 6].

In our previous studies [7-9] a series of synthetic binary, ternary and multicomponent mixtures were designed as simple model fluids for real HPHT reservoir fluids. These mixtures include

methane/n-decane, methane/n-butane/n-decane, methane/n-butane/n-dodecane and methane/n-butane/n-hexane/n-decane/n-hexadecane/n-eicosane, and their compositions were designed to represent either volatile oils or gas condensates. Their volumetric properties and phase equilibria were experimentally determined in broad temperature and pressure ranges. We also compared the measured properties with predictions from different equations of state (EoSs), including Soave-Redlich-Kwong (SRK) [10], Peng-Robinson (PR) [11], Soave-Benedict-Webb-Rubin (S-BWR) [12], and Perturbed-Chain Statistical Association Fluid Theory (PC-SAFT) [13]. The comparison involves systems of different composition characteristics and various properties, and it is impossible to single out a model that performs always better than the others in all cases. Nevertheless, for saturation pressures, SRK, PR and PC-SAFT are similar while S-BWR tends to give significantly different phase envelopes for very asymmetric mixtures; for single-phase densities, PC-SAFT and S-BWR are generally better while PC-SAFT's performance seems to be more stable among the synthetic mixtures tested.

In the present work we extend our previous studies to two real reservoir fluids, one HPHT volatile oil and one HPHT gas condensate. We determined experimentally their densities, isothermal compressibilities, saturation pressures, and liquid fractions in the two-phase region in the temperature range from (298.15 to 473.15)K (the density and compressibility determined up to 463.15 K). A high pressure vibrating tube densitometer from Anton Paar was used for density determinations up to 140 MPa, and the study of phase equilibrium was carried out in a PVT cell from Sanchez Technologies. In the modelling part, we used the aforementioned EoSs except for S-BWR because S-BWR tends to predict very different saturation pressures for asymmetric mixtures. For SRK and PR, we also included the calculation with volume translation in order to improve their density calculation results. To apply these EoSs to reservoir fluids, appropriate characterization of their C_7^+ fractions was also performed. We analysed and

compared the model performance for the prediction of volumetric properties and phase behaviour.

2. Materials and methods

2.1. Materials

Both the HPHT volatile oil sample and the HPHT gas condensate sample are bottom hole samples taken from HPHT reservoirs in the Danish North Sea. The samples were received in high pressure cylinders at ambient temperature and pressures of 48 MPa and 93 MPa for the volatile oil and the gas condensate, respectively. The received volatile oil and gas condensate samples were kept at constant pressure and conditioned at 366 K and 363 K, respectively. In order to determine the composition of the reservoir fluids, a separator test was performed for each fluid. The compositional analysis of the obtained gas and oil phases was performed through a gas chromatograph Agilent 7890A gas. The compositional data, together with the gravimetrical and volumetric measurements at ambient pressure allowed to establish the overall composition of the reservoir fluids along with their gas oil ratio (GOR), which is defined as the ratio of the gas volume to the oil volume of a reservoir sample at 0.1013 MPa and 288.75 K. Two replicates of the separator test were performed for each reservoir fluid.

The obtained composition of the reservoir fluids is presented in Table 1 for the HPHT volatile oil and the HPHT gas condensate. The volatile oil has a methane mole fraction of 49.3% whereas the methane mole fraction of the gas condensate is 82.7%, as concerns the mole fraction of C_7^+, it is 27.76% and 4.2% for the HPHT volatile oil and HPHT gas condensate, respectively.

Table 1
Compositional analysis (mole fraction %) and molecular weight of the HPHT reservoir fluids to C_{36}^+.

Component	HPHT Volatile oil	HPHT Gas condensate
CO_2	0.14	2.40
N_2	1.41	0.10
C_1	49.3	82.7

C_2	9.78	6.43
C_3	4.67	2.34
iC_4	0.62	0.38
C_4	1.32	0.65
iC_5	0.22	0.19
C_5	2.96	0.26
C_6	1.82	0.35
C_7	3.05	0.67
C_8	3.46	0.93
C_9	2.69	0.61
C_{10}	2.30	0.40
C_{11}	1.40	0.20
C_{12}	2.30	0.25
C_{13}	3.19	0.20
C_{14}	1.57	0.16
C_{15}	0.96	0.11
C_{16}	0.88	0.11
C_{17}	0.65	0.07
C_{18}	0.56	0.06
C_{19}	0.40	0.05
C_{20}	0.37	0.04
C_{21}	0.40	0.04
C_{22}	0.37	0.04
C_{23}	0.32	0.03
C_{24}	0.30	0.03
C_{25}	0.26	0.02
C_{26}	0.24	0.02
C_{27}	0.21	0.02
C_{28}	0.20	0.02
C_{29}	0.17	0.01
C_{30}	0.16	0.01
C_{31}	0.14	0.01
C_{32}	0.13	0.01
C_{33}	0.11	0.01
C_{34}	0.10	0.01
C_{35}	0.09	0.01
C_{36}^+	0.78	0.05
Molecular weight	70.8	25.2

As concerns the gas oil ratio (GOR), it was found to be 224 Sm^3/Sm^3 for the HPHT volatile oil and 2654 Sm^3/Sm^3 for the HPHT gas condensate, where Sm^3/Sm^3 stands for standard cubic meters of gas at 0.1013 MPa and 288.75 K per cubic meter of stock tank oil (STO) at the same conditions. The measured densities of the stock tank oil at 0.1013 MPa and 288.75 K were 0.8012 and 0.8001 $g \cdot cm^{-3}$ for the HPHT volatile oil STO and the HPHT gas condensate STO, respectively. More details about the C_7^+ and C_{36}^+ fractions of the reservoir fluids are given in Table 2. For the volatile oil the density of the C_7^+ fraction was obtained from the density measurements of the STO and the C_6 fraction (obtained from true boiling point distillation), whereas the C_{36}^+ density was obtained by using the single carbon number densities previously

reported by Katz and Firoozabadi [14] (extrapolated to C_{72} fraction) together with the STO mass fractions of the volatile oil measured with GC up to C_{72}. As concerns the gas condensate, the densities of the C_7^+ and the C_{36}^+ fractions were obtained by combining the compositional data we have measured from the separator oil up to C_{72} with the density of the single carbon numbers reported by Katz and Firozobadi [14] (extrapolated to C_{72} fraction).

Table 2
Molecular weight and density of the C_7^+ and C_{36}^+ fractions.

Fluid	Fraction	Mole fraction %	Molecular weight	ρ^* /g·cm^{-3}
HPHT volatile oil	C_7^+	27.76	189.4	0.8076
	C_{36}^+	0.78	611.6	0.9367
HPHT gas condensate	C_7^+	4.20	162.4	0.8008
	C_{36}^+	0.05	593.7	0.9339

*Density at 288.75 K and 0.1 MPa

2.2. Density measurements

The experimental determination of the density was carried out by using a high pressure vibrating tube densitometer DMA HPM from Anton Paar. In this apparatus, the oscillation period of a U-tube filled with the sample is measured and displayed with 7 significant figures. The calibration of the device was performed from (298.15 to 463.15)K and pressures up to 140 MPa, following a modified Lagourette et al. method [15, 16] which uses vacuum, Milli-Q water and n-dodecane as reference fluids. After calibration, the density of the studied samples was obtained from the oscillation period measurements. The density determination was performed for the reservoir fluids in the single phase, i.e. the measurements were performed at pressures higher than the saturation pressure (p^{sat}). The uncertainty of the density through this technique has been rigorously calculated by Segovia et al. [17]. In the present work the expanded (k=2) uncertainty of the density measurements is considered to be $7 \cdot 10^{-4}$ g·cm^{-3} at T<373.15K and $3 \cdot 10^{-3}$ g·cm^{-3} at other temperature conditions.

The pressure was generated in the vibrating tube densitometer through a pressure line comprised of high pressure pipes and valves and a high pressure generator (HiP 37-6-30). The

pressure was measured by using a pressure transducer SIKA type P that can measure pressure up to 150 MPa with a 0.05% FS uncertainty. As concerns temperature control, it was performed by means of a liquid circulator bath Julabo PRESTO A30 and the temperature was measured through a Pt-100 located inside the measurement cell with an uncertainty of ±0.02 K. A schematic of the complete setup for the density measurements has been previously published [7].

2.3. Phase equilibrium measurements

The measurement of the phase equilibrium was performed in a PVT cell PVT 240/1500 FV with full visibility from Sanchez Technologies. The measurements can be performed in the temperature range up to 473.15 K and pressures up to 150 MPa. This apparatus consists of a stainless steel hollow cylinder with a motor driven piston in one end and a sapphire window in the other end. The motor driven piston is used to change the pressure inside the PVT cell by increasing or decreasing the cell volume, the maximum volume of the cell is 240 cm^3. A stirring system composed of four retractable blades is located in the head of the piston and driven by a motor through a magnetic coupling, this stirring system is used to homogenize the studied sample. The full visibility of the cell is achieved through a CCD digital camera Lumenera Lw1335C located in front of the sapphire window together with a set of two lamps connected to four optical fibers. The cell has a rocking mechanism that allows its rotation to a certain angle depending on the type of fluid under study. The whole apparatus is computer controlled through the Falcon Software. A schematic of the experimental setup has been published elsewhere [9].

As concerns the temperature control, it is performed through a set of 8 electrical resistances located in the wall of the cell. Additionally, a liquid circulating thermostat Julabo Presto A40 is connected to a jacket covering the cell, the thermostating liquid circulates with a temperature set point 5 K lower than the sample temperature in order to improve the temperature stability

of the system. The temperature is measured by using a Pt-100 located in the wall of the cell with an uncertainty of ±0.02 K. Regarding pressure, a pressure transducer Dynisco PT435A inserted in the wall of the cell is used for the pressure measurements, this pressure transducer is newly calibrated against a reference pressure transducer, as a function of temperature and pressure, prior to the loading of a new sample in the PVT cell. The pressure standard uncertainty is 0.06 MPa.

The experimental determination of the saturation pressure was performed through visual observation. The pressure was slowly decreased at constant temperature from the single phase with a constant flow rate of $1.4 \cdot 10^{-4}$ or $2.8 \cdot 10^{-4}$ $cm^3 \cdot s^{-1}$ under continuous stirring until the appearance of a new phase was observed, at this point the pressure reading indicated the saturation pressure and it was recorded. Each determination was performed by triplicate for both reservoir fluid samples at selected temperatures covering the range from (298.15 to 473.15)K. The combined standard uncertainty of the determination of the equilibrium pressure is estimated to be 0.10 MPa for bubble points and 0.15 MPa for dew points. This uncertainty was estimated by combining the standard uncertainty of the pressure readings with the repeatability of the visual determinations of saturation pressure.

A constant mass expansion (CME) procedure was applied to both reservoir fluid samples at selected temperatures in the range from (298.15 to 473.15)K. This procedure was performed automatically through the Falcon Software. The measurements started from the single phase sample at constant temperature, a series of pressure steps were made in the single phase region, in each of them the sample was stirred for a certain period (at least 60 s) and after this a set of waiting periods of 600 s were applied until a pressure stability (±0.05 MPa) was achieved. After stabilization, the pressure and volume of the system were recorded and a photo of the sample was taken through the Euclide software version 1.4.2. Once the saturation pressure was reached through the aforementioned pressure steps, a series of volume steps were performed

in the two phase region. Equilibrium pressure and volume were also recorded for each step, as well as a photo of the sample. Afterwards, the liquid fraction percentage in the two phase region was measured from the photos by using the Euclide software, which based on geometrical relations determines the liquid volume for each of the steps. The maximum standard uncertainty of the liquid fractions reported in this work is 2.1%.

2.4. Modelling

The experimental data measured in this work have been modelled by using two cubic equations of state (EoSs), Soave-Redlich-Kwong (SRK), and Peng-Robinson (PR) and a non-cubic EoS, Perturbed Chain Statistical Associating Fluid Theory (PC-SAFT) [13, 18]. For the last EoS, its simplified version described by von Solms et al. [13] was used in the calculations.

In the volumetric calculations, the Peneloux [19] volume correction (c) can be applied to the cubic EoSs in order to compensate for their poor density prediction. The volumes calculated by the cubic EoSs (V_{SRK} and V_{PR}) are related to the volumes calculated by the volume translation EoSs (SRK-VT and PR-VT) through the volume correction parameter of SRK (c_{SRK}) and PR (c_{PR}), as follows:

$$V_{SRK-VT} = V_{SRK} - c_{SRK} \tag{1}$$

$$V_{PR-VT} = V_{PR} - c_{PR} \tag{2}$$

where $V_{\mathrm{SRK\text{-}VT}}$ and $V_{\mathrm{PR\text{-}VT}}$ are the molar volumes calculated with SRK and PR with volume translation, respectively, V_{SRK} and V_{PR} are the molar volumes calculated with SRK and PR, respectively, and c_{SRK} and c_{PR} are the Peneloux volume correction for SRK and PR, respectively.

The Peneloux volume correction is calculated according to the following equation for both SRK (c_{SRK}) and PR (c_{PR}):

$$c = \sum_i x_i c_i \tag{3}$$

where x_i is the mole fraction of the single carbon number C_i and c_i is the Peneloux volume correction of the single carbon number C_i.

For single carbon number components with carbon number smaller than 7, their Peneloux volume corrections are calculated by equations 4 and 5 for SRK and PR, respectively [20]:

$$c_{SRK} = \frac{0.40768 R T_c \left(0.29441 - Z_{RA}\right)}{p_c} / cm^3 mol^{-1} \tag{4}$$

$$c_{PR} = \frac{0.50033 R T_c \left(0.25969 - Z_{RA}\right)}{p_c} / cm^3 mol^{-1} \tag{5}$$

where R is the universal gas constant, T_c is the critical temperature, p_c is the critical pressure and Z_{RA} (Rackett compressibility factor) is given by the following equation [21]:

$$Z_{RA} = 0.29056 - 0.08775\omega \tag{6}$$

where ω is the acentric factor.

For components in C_7^+, their shift parameters were obtained through characterization by matching the density of C_7^+. In this sense, the density calculation for SRK and PR with volume translation has involved certain adjustment to experimental data although in an indirect manner. For the characterization of the C_7^+ fraction of the reservoir fluid samples, we used the methods described by Yan et al. [22] and Varzandeh et al. [3] which are based on the characterization method of Pedersen et al. [23, 24]. The difference from the method of Pedersen et al. lies in how the model parameters are estimated. The first step of characterization is the same for all EoS models: an exponential distribution was used for the calculation of mole fraction of the single carbon number (SCN) components in the plus fraction. In the second step, the parameter estimation for SRK and PR was performed by using Twu's correlation [25] for p_c and T_c and

Lee-Kesler correlation [26] for ω. For PC-SAFT, the correlations of Varzandeh et al. [3] were used to calculate the model parameters. In the last step the SCN components were lumped into a few pseudo-components with approximately equal mass.

The single compound model parameters as well as those for the lumped components are presented in tables A.1 and A.2 from the supplementary material. The binary interaction parameters, k_{ij}, used in this work and the mixing rules are provided in tables A.3 and A.4 of the supplementary material.

An in-house calculation code [3, 22] was used for all the calculations. In principle, group contribution based characterization methods such as the method of Skjold-Jørgensen [27] could also be used for characterization. But they require additional information for chemical groups which are usually not available from the chemical analytical data. The classical C_7^+ characterization based on boiling points and fraction densities is therefore more appropriate here. Regarding the selection of EoS models, we include two cubics and one non-cubic with strong theoretical basis. But we have not included the association model like the cubic plus association (CPA) model [28] here. This is because the CPA model reduces to SRK for systems without associating components and the calculation is essentially SRK with a different set of parameters [28]. The application of CPA with reservoir fluids and associating compounds can be found in Yan et al. [29]

3. Results and discussion

In the present work, the comparison between the experimental data and the model predictions is performed through the absolute average deviation (AAD), the absolute average relative deviation (AARD) and the standard deviation (σ), which are defined as follows:

$$\mathrm{AAD} = \frac{1}{N}\sum_{i=1}^{N}\left|Y_i^{cal} - Y_i^{\exp}\right| \tag{7}$$

$$\mathrm{AARD}/\% = \frac{100}{N}\sum_{i=1}^{N}\left|\frac{Y_i^{cal} - Y_i^{\exp}}{Y_i^{\exp}}\right| \tag{8}$$

$$\sigma = \sqrt{\frac{\sum_{i=1}^{N}\left(Y_i^{\exp} - Y_i^{cal}\right)^2}{N-p}} \tag{9}$$

where $Y_i^{\exp}$is the value of the experimental property determined in this work, Y_i^{cal} is the value predicted through the model for the same property, N is the number of experimental data points and p is the number of fitting parameters. In the comparison of density-related properties, the original SRK and PR, their volume translated versions, and PC-SAFT are included. However, volume-translated SRK and PR are excluded in the calculation of saturation pressures since volume translation does not affect phase equilibrium.

3.1. Density

The experimental density data of the two HPHT reservoir fluids in the studied temperature and pressure range is gathered in Table 3. Under the studied conditions, the density of the HPHT volatile oil varies in the range (0.54 to 0.74) g·cm^{-3} whereas the density of the HPHT gas condensate varies in the range (0.30 to 0.50) g·cm^{-3}. The expected trends of density with temperature and pressure were found, i.e. density increases with pressure along isotherms, whereas it decreases with temperature along isobars.

Table 3
Experimental density data[a], ρ, of the HPHT reservoir fluids in g·cm^{-3}.

T/K	p/MPa					
	40.00	60.00	80.00	100.00	120.00	140.00
			HPHT volatile oil			
298.15	0.6781	0.6945	0.7080	0.7197	0.7301	0.7393
323.15	0.6579	0.6768	0.6918	0.7047	0.7161	0.7261
348.15	0.6374	0.6590	0.6758	0.6899	0.7021	0.7129
358.15	0.6279	0.6505	0.6680	0.6826	0.6950	0.7062
373.15	0.6153	0.6395	0.6581	0.6734	0.6865	0.6980
423.15	0.5755	0.6060	0.6284	0.6463	0.6614	0.6745
432.15	0.5685	0.6002	0.6233	0.6417	0.6572	0.6707
463.15	0.5433	0.5799	0.6056	0.6258	0.6426	0.6570

			HPHT gas condensate			
298.15	–	–	0.4476	0.4681	0.4848	0.4987
323.15	–	–	0.4288	0.4510	0.4689	0.4839
348.15	–	0.3781	0.4107	0.4346	0.4536	0.4694
363.15	–	0.3649	0.3986	0.4236	0.4434	0.4599
373.15	–	0.3577	0.3930	0.4189	0.4392	0.4560
393.15	–	0.3435	0.3809	0.4082	0.4294	0.4466
423.75	–	0.3226	0.3621	0.3911	0.4135	0.4316
463.15	–	0.2962	0.3384	0.3693	0.3925	0.4112

[a]Expanded density uncertainty $U(\rho)$ (k=2): $0.7 \cdot 10^{-3}$ g·cm^{-3} at $T < 373.15$ K; $3 \cdot 10^{-3}$ g·cm^{-3} at other temperature conditions; standard temperature uncertainty $u(T)$: 0.02 K; standard pressure uncertainty $u(p)$: 0.08 MPa.

The experimental density data for both reservoir fluids have been correlated as a function of temperature and pressure by using the following modified Tammann-Tait equation:

$$\rho(T,p) = \frac{\rho(T,p_{ref})}{1 - C \cdot \ln\left(\frac{B(T)+p}{B(T)+p_{ref}}\right)} \tag{10}$$

where $\rho(T, p_{ref})$ is the density in g·cm^{-3} as a function of temperature (K) at a reference pressure (MPa), given by the following equation:

$$\rho(T,p_{ref}) = \sum_{i=0}^{3} A_i T^i \tag{11}$$

C is a temperature and pressure independent parameter and $B(T)$ is a temperature dependent parameter given by:

$$B(T) = \sum_{j=0}^{2} B_j T^j \tag{12}$$

The fitting parameters of Equation 10 are given in Table 4 together with σ and σ^*, which are the standard deviations for Equations 11 and 10, respectively. The absolute average relative deviation of the fit is also provided.

Table 4
Modified Tammann-Tait (Equation 10) parameters for the HPHT volatile oil and the HPHT gas condensate. σ is the standard deviation for Equation (11) and σ^* the standard deviation for equation (10).

	HPHT volatile oil	HPHT gas condensate

p_{ref} / MPa	40	60
A_0 /g·cm^{-3}	0.9434	0.8736
$10^4 \cdot A_1$ /g·cm^{-3}·K^{-1}	-9.35	-22.95
$10^7 \cdot A_2$ /g·cm^{-3}·K^{-2}	1.53	32.12
$10^9 \cdot A_3$ /g·cm^{-3}·K^{-3}	—	-2.046
$10^3 \cdot \sigma$/ g·cm^{-3}	0.6	0.7
C	0.1024	0.145
B_0 /MPa	280.7	117.34
B_1 /MPa·K^{-1}	-1.1244	-0.6568
$10^3 \cdot B_2$ /MPa·K^{-2}	1.0	0.66
$10^3 \cdot \sigma^*$ / g·cm^{-3}	0.7	0.9
AARD / %	0.08	0.16

The experimental density values are plotted in Fig. 1 at selected temperatures together with modelling results. A quantitative comparison of the model performance for density prediction is shown in Fig. 2, where it can be observed that the best density prediction for the volatile oil is obtained through the cubic EoSs with volume translation and PC-SAFT, these three EoSs provided similar deviations in the density predictions. Regarding the gas condensate, the best density prediction was obtained through PR-VT closely followed by PC-SAFT and SRK-VT. The worst density predictions were given by the cubic EoSs without volume translation, SRK and PR. For the two HPHT reservoir fluids studied here, simple cubic EoSs with volume translation can achieve similar performance for density prediction to the advanced thermodynamic model PC-SAFT which has a more theoretical background in statistical mechanics.

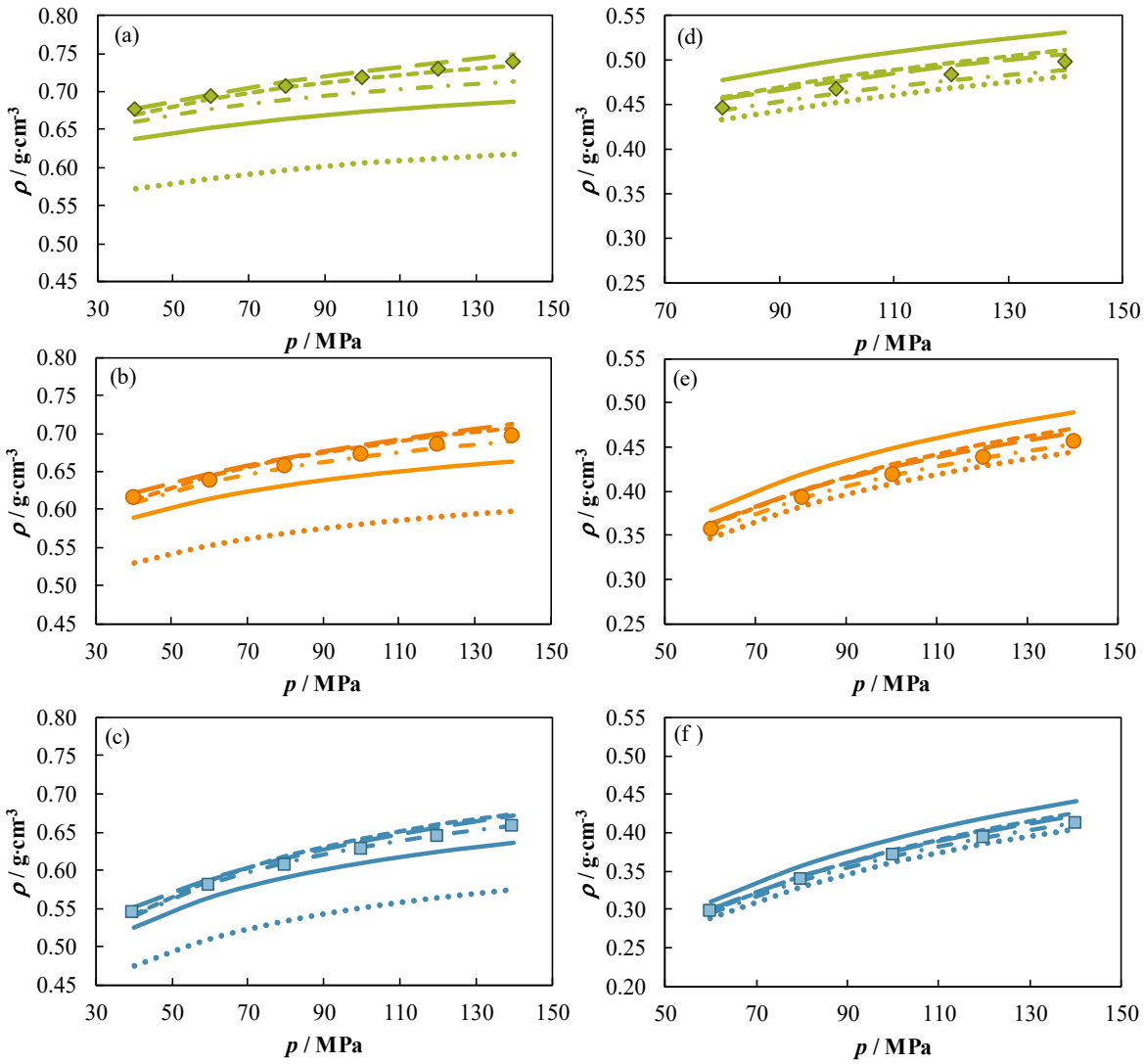

Fig. 1. Experimental density data, ρ, at 298.15 K (◆), 373.15 K (●) and 463.15 K (■) for the HPHT volatile oil (a, b, c) and for the HPHT gas condensate (d, e, f). Lines represent the model predictions SRK (•••), SRK-VT (– – –), PR (—), PR-VT (– • –) and PC-SAFT (— —).

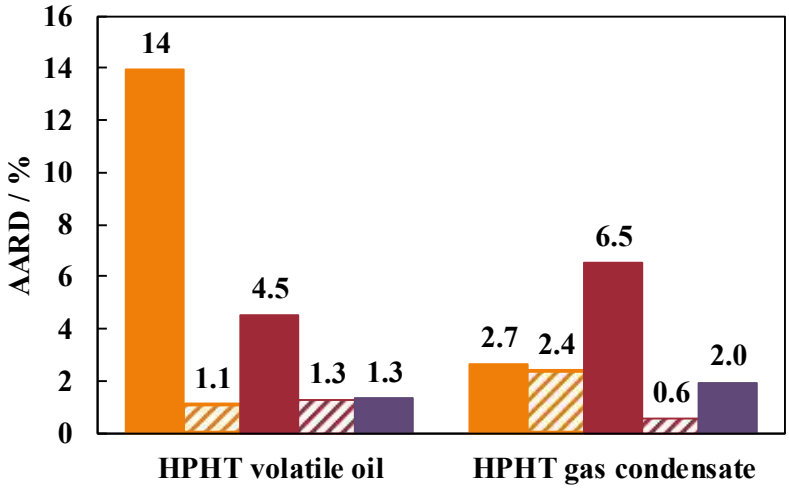

Fig. 2. Absolute average relative deviations of the density predictions for the HPHT volatile oil and the HPHT gas condensate through SRK (solid orange), SRK-VT (striped orange), PR (solid red), PR-VT (striped red) and PC-SAFT (solid purple).

3.2. Isothermal compressibility

The isothermal compressibility values (κ_T) of the two reservoir fluids were obtained by differentiation from the modified Tammann-Tait fitting (Equation 10) according to the following equation:

$$\kappa_T(T,p) = \frac{1}{\rho}\left(\frac{\partial \rho}{\partial p}\right)_T \tag{13}$$

The isothermal compressibility values of the two fluids studied in this work are presented in Table 5, whereas the compressibility is plotted against pressure together with model predictions at selected temperatures in Fig. 3. A quantification of the model performance for prediction of isothermal compressibility is presented in Fig. 4, where it is observed that even though PC-SAFT provides a slightly better prediction, the predictions of this property for the HPHT volatile oil are very similar for the different models, with average deviations around 10%. Concerning the HPHT gas condensate, the compressibility predictions are better than the ones obtained for the volatile oil, with AARD lower than 9%. The best prediction for this fluid was obtained with PC-SAFT with an AARD of 4.4 %.

Table 5
Isothermal compressibility values[a], $10^3 \kappa_T$ (MPa^{-1}), of the HPHT reservoir fluids.

T/K	p/MPa			
	60.00	80.00	100.00	120.00
	HPHT volatile oil			
298.15	1.07	0.91	0.79	0.70
323.15	1.22	1.02	0.87	0.76
348.15	1.40	1.14	0.96	0.83
358.15	1.48	1.19	1.00	0.86
373.15	1.61	1.27	1.06	0.91
423.15	2.11	1.57	1.26	1.06
432.15	2.21	1.63	1.30	1.09
463.15	2.55	1.81	1.42	1.18
	HPHT gas condensate			
298.15	—	2.58	2.03	1.68
323.15	—	2.91	2.23	1.83
348.15	—	3.27	2.45	1.98
363.15	—	3.50	2.58	2.07
373.15	—	3.66	2.67	2.13
393.15	—	3.98	2.85	2.25
423.75	—	4.46	3.11	2.43
463.15	—	4.93	3.36	2.60

[a]Relative expanded isothermal compressibility uncertainty $U_r(\kappa_T)$ (k=2): 0.013

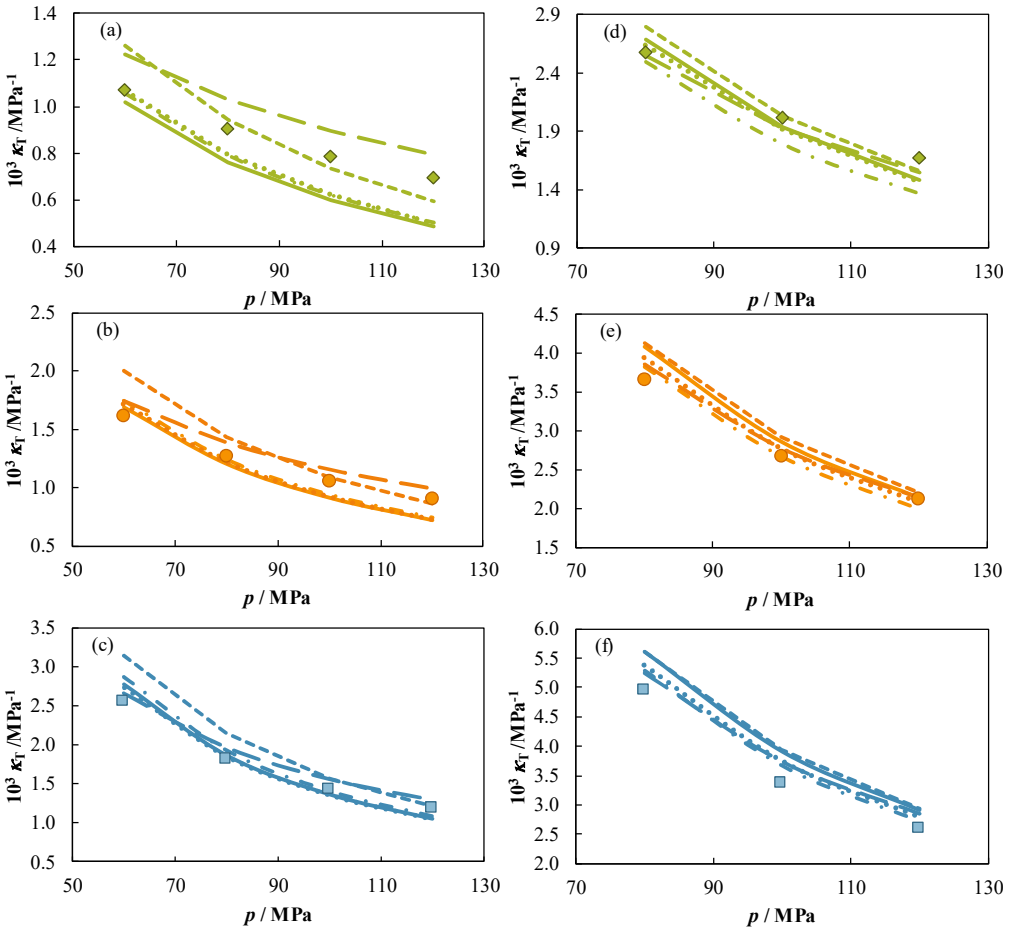

Fig. 3. Experimental compressibility data, κ_T, at 298.15 K (◆), 373.15 K (●) and 463.15 K (■) for the HPHT volatile oil (a, b, c) and for the HPHT gas condensate (d, e, f). Lines represent the model predictions SRK (•••), SRK-VT (– – –), PR (——), PR-VT (– • –) and PC-SAFT (—— ——).

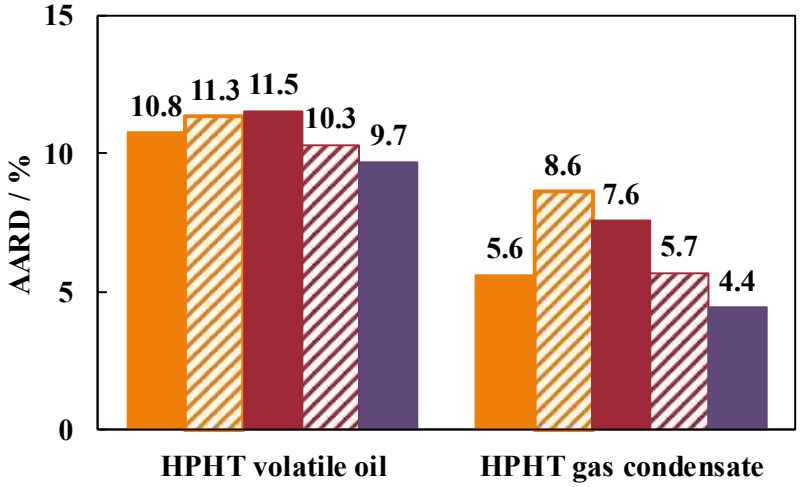

Fig. 4. Absolute average relative deviations of the isothermal compressibility predictions for the HPHT volatile oil and the HPHT gas condensate through SRK (solid orange), SRK-VT (striped orange), PR (solid red), PR-VT (striped red) and PC-SAFT (solid purple).

Recently, Burgess et al. [30] published experimental data and analyzed the predictive capability of PC-SAFT and SRK-VT for density and isothermal compressibility of two crude oils and their synthetic mixtures with methane at HPHT conditions (pressures up to 276 MPa and temperatures up to 523 K). They used only three pseudo-components to represent the crude oil together with a set of high pressure parameters, and their prediction of density values was within 1-4%, whereas the prediction of isothermal compressibility was within 1-10%, which is in agreement with the predictions of density and isothermal compressibility obtained in the present work for real reservoir fluids. However, when they used Gross and Sadowski [18] parameters for PC-SAFT, instead of the high pressure parameters, the compressibility prediction was within 40%, in contrast to the present work where we get a good prediction of compressibility values (maximum deviation 14.2%) with these last parameters. These authors [30] reported also poor predictions of the isothermal compressibility by using SRK with volume translation at all p,T conditions with deviations reaching in some points more than 50%, in contrast to the present work where the maximum average deviations of cubic EoSs with volume translation for isothermal compressibility are around 10%, with maximum deviations of 27%.

3.3. Phase equilibrium

The measured saturation pressures (p^{sat}) for the HPHT reservoir fluids are presented in Table 6. In the studied temperature range a maximum saturation pressure of 26.34 MPa was measured for the HPHT volatile oil at 432.12 K, whereas for the HPHT gas condensate a maximum saturation pressure of 69.55 MPa was measured at 298.15 K. These experimental data are plotted together with the different model predictions for this property in Fig. 5. The plot of the saturation pressure of the HPHT gas condensate against temperature is similar to the one previously reported by Ungerer et al. [31] for a high pressure natural gas where high dew pressures up to 70 MPa were reported and attributed to the simultaneous abundance of methane

and significant amount of heavy hydrocarbons in the sample. In this last figure, it can also be observed that the models that reproduce better the experimental data are SRK and PR for the HPHT volatile oil and PC-SAFT for the HPHT gas condensate. A quantitative analysis of the model deviations is presented in Fig. 6 where, as already observed in Fig. 5, it is shown how the simple cubic EoSs perform better than PC-SAFT in the prediction of the saturation pressure of the HPHT volatile oil, the opposite trend was found for the HPHT gas condensate where PC-SAFT provides better prediction. Among the three models studied in this work it is not possible to find one that performs equally well for the two HPHT reservoir fluids analysed in the present work without tuning of binary interaction factors, k_{ij}.

Table 6
Saturation pressure[a], p^{sat}, of the HPHT reservoir fluids studied in this work.

T / K	p^{sat} / MPa	T / K	p^{sat} / MPa
HPHT volatile oil		HPHT gas condensate	
298.06	20.92	298.15	69.55
323.13	22.65	323.15	64.41
348.00	24.20	348.15	59.57
358.10	24.64	363.16	57.32
373.08	25.24	372.93	56.17
398.02	25.94	393.18	53.92
423.09	26.29	413.20	51.88
432.12	26.34	423.79	50.87
448.00	26.32	433.15	49.81
473.04	26.03	447.97	48.27
		473.15	45.60

[a]Standard temperature uncertainty $u(T)$: 0.02 K; Combined standard pressure uncertainty $u(p)$:0.10 MPa for the HPHT volatile oil and 0.15 MPa for the HPHT gas condensate.

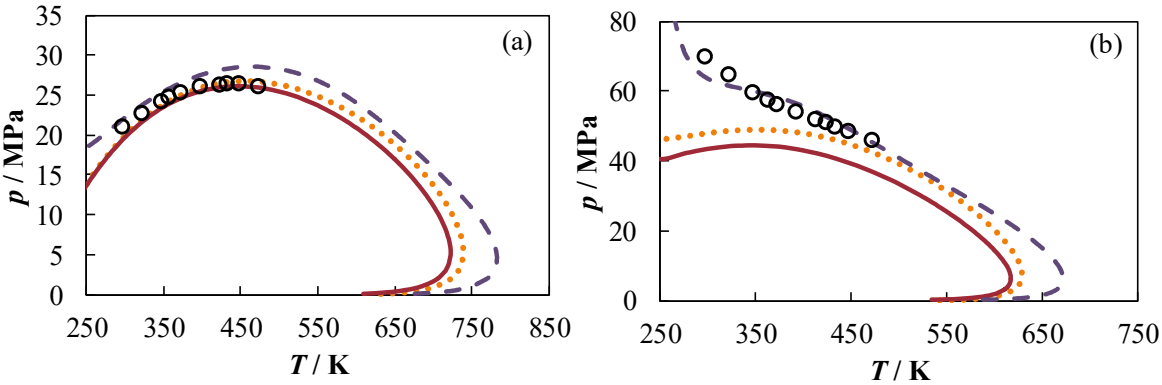

Fig. 5. Experimental saturation pressure (O) of (a) HPHT volatile oil and (b) HPHT gas condensate. Lines represent the model predictions SRK (•••), PR (—) and PC-SAFT (– –).

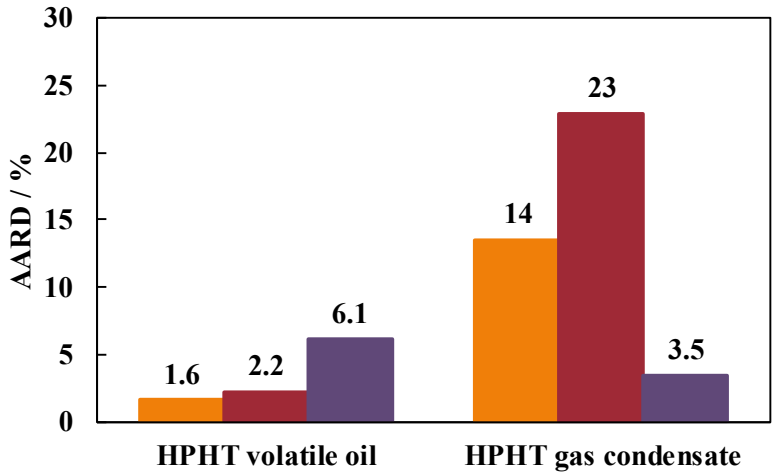

Fig. 6. Absolute average relative deviations obtained in the prediction of the experimental saturation pressure for the HPHT volatile oil and for the HPHT gas condensate through SRK (orange), PR (red) and PC-SAFT (purple).

An example of the images of the PVT cell in the two-phase region during the CME process is presented in Fig. 7 and in Fig. 8. These pictures were used to determine the liquid fraction percentage ($100 \cdot V_{liq}/V_{tot}$), i.e. the ratio between the liquid volume and the total volume at given p, T conditions below the saturation pressure. The yellow line in Fig. 7 indicates the level of the vapour-liquid interface in contact with the sapphire window of the PVT cell, as the experiments were performed in a cell positioning angle of 45°, the vapour-liquid interface can be also observed in contact with the head of the cell piston. The results for the constant mass expansion (CME) procedure are gathered in Tables 7 and 8 for the HPHT volatile oil and the HPHT gas condensate, respectively. Measurements of the liquid fraction percentage and the relative volume (V_{tot}/V_{sat}),which is the ratio between the total volume and the volume at saturation pressure at given T are presented in these tables.

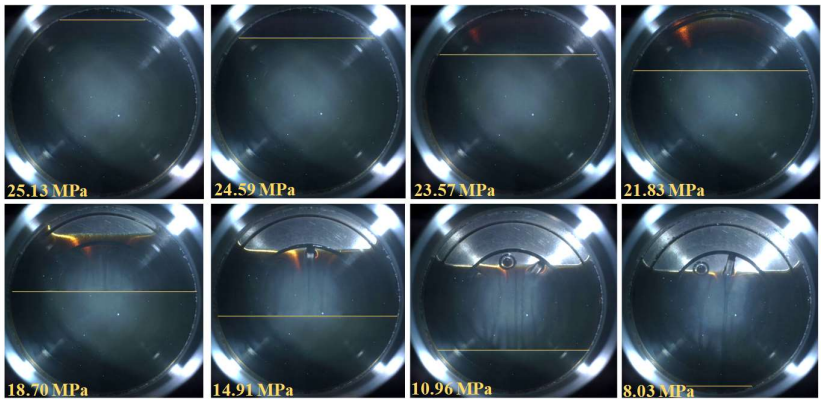

Fig. 7. Pictures showing the liquid fraction in the CME experiment of the HPHT volatile oil at 373.15 K. The yellow line represents the liquid level. PVT cell positioning angle: 45°.

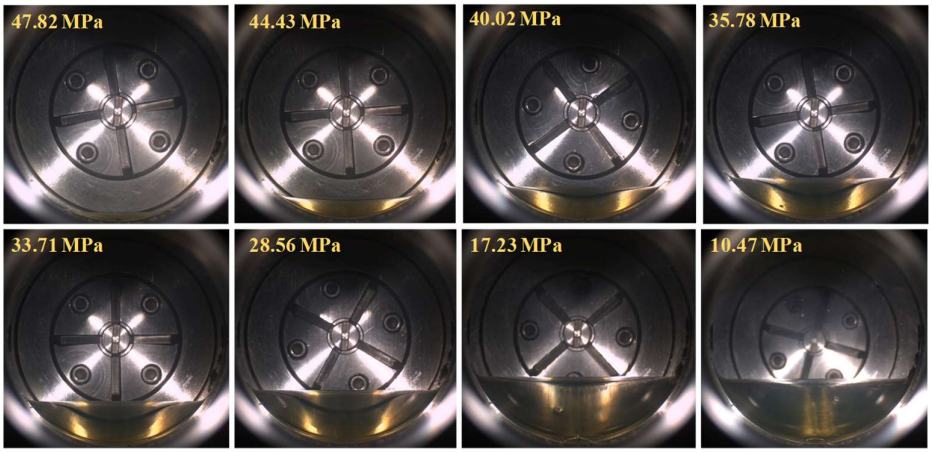

Fig. 8. Pictures showing the liquid fraction in the CME experiment of the HPHT gas condensate at 393.15 K. PVT cell positioning angle: 315°.

Table 7
Liquid fraction percentage ($100 \cdot V_{liq}/V_{tot}$) and relative volume ($V_{tot}/V_{sat}$) for the HPHT volatile oil.[a]

p	%		p	%		p	%		p	%	
MPa	V_{liq}/V_{tot}	V_{tot}/V_{sat}	MPa	V_{liq}/V_{tot}	V_{tot}/V_{sat}	MPa	V_{liq}/V_{tot}	V_{tot}/V_{sat}	MPa	V_{liq}/V_{tot}	V_{tot}/V_{sat}
T=298.15 K			T=323.15 K			T=358.15 K			T=373.15 K		
51.79	0.939		53.71	0.930		51.63	0.923		52.59	0.917	
51.12	0.940		52.47	0.932		51.22	0.924		51.82	0.919	
49.34	0.944		50.80	0.935		49.43	0.929		50.22	0.922	
47.53	0.947		49.17	0.938		47.51	0.933		48.25	0.926	
45.41	0.950		46.96	0.942		45.39	0.938		46.34	0.931	
43.38	0.953		45.16	0.946		43.47	0.943		44.32	0.937	
41.51	0.956		42.93	0.950		41.37	0.948		42.46	0.941	
39.60	0.960		41.02	0.954		39.50	0.953		40.46	0.947	
37.41	0.964		39.26	0.957		37.42	0.958		38.45	0.952	
35.50	0.968		37.11	0.962		35.42	0.964		36.43	0.958	
33.47	0.972		35.14	0.967		33.53	0.969		34.38	0.965	
31.67	0.975		33.29	0.971		31.51	0.976		32.43	0.971	
29.62	0.980		31.19	0.976		29.44	0.982		30.36	0.978	
27.45	0.984		29.22	0.981		27.38	0.989		28.46	0.985	
25.49	0.989		27.11	0.986		25.42	0.997		28.21	0.986	
23.34	0.994		25.17	0.992		25.27	0.997		26.39	0.994	
21.32	0.999		23.23	0.998		25.25	0.997		26.26	0.994	

21.05		0.999	23.06		0.998	24.78		0.999	26.13		0.995
21.02		0.999	22.94		0.998	24.45	99.49	1.003	26.13		0.995
20.70		1.001	22.57		1.000	23.87	97.75	1.011	25.74		0.997
20.39		1.005	22.28	99.33	1.004	22.77	94.39	1.029	25.13	99.83	1.000
19.63	97.76	1.015	21.62	97.69	1.013	20.99	88.99	1.064	24.59	97.97	1.009
18.33	94.76	1.033	20.39	94.69	1.031	17.85	79.14	1.152	23.57	94.43	1.026
16.45	90.14	1.071	18.53	89.98	1.068	14.15	66.84	1.327	21.83	89.09	1.060
13.61	81.06	1.166	15.47	80.48	1.160	10.37	51.99	1.677	18.70	78.58	1.146
10.65	68.76	1.356	12.13	68.30	1.344	7.58	39.63	2.202	14.91	66.40	1.317
7.77	53.56	1.735	8.85	52.77	1.712				10.96	51.73	1.659
5.69	40.28	2.303	6.46	39.74	2.263				8.03	38.57	2.172
T=423.15 K			*T*=432.15 K			*T*=473.15 K					
52.33		0.888	51.32		0.892	50.80		0.862			
51.05		0.891	50.46		0.894	50.03		0.864			
49.32		0.897	48.82		0.899	48.27		0.870			
47.29		0.902	46.80		0.905	46.30		0.877			
45.33		0.909	44.84		0.911	44.33		0.885			
43.42		0.914	42.88		0.918	42.35		0.893			
41.46		0.921	40.91		0.925	40.38		0.902			
39.39		0.929	38.93		0.933	38.34		0.912			
37.43		0.937	36.86		0.941	36.39		0.922			
35.42		0.944	34.83		0.950	34.39		0.934			
33.47		0.953	32.94		0.960	32.39		0.947			
31.43		0.963	30.84		0.971	30.41		0.961			
29.40		0.974	28.92		0.982	28.39		0.978			
29.23		0.975	28.77		0.983	28.25		0.978			
27.38		0.986	26.88		0.996	26.37		0.997			
27.27		0.987	26.69		0.997	26.28		0.998			
27.11		0.988	26.51		0.998	26.16		0.999			
27.00		0.988	26.43		0.999	25.96	99.71	1.002			
26.77		0.990	26.28		1.001	25.64	96.46	1.009			
26.32		0.993	26.13	98.88	1.004	25.02	90.93	1.023			
25.85	97.77	1.001	25.74	96.67	1.011	23.90	83.49	1.052			
25.04	93.72	1.017	24.95	92.53	1.027	21.56	72.14	1.122			
23.60	87.50	1.048	23.59	86.19	1.058	18.18	59.59	1.264			
20.75	76.76	1.126	20.87	75.87	1.135	14.06	45.95	1.547			
16.98	63.86	1.282	17.20	63.03	1.290						
12.75	49.10	1.595	12.99	48.25	1.599						

[a]Standard temperature uncertainty $u(T)$: 0.02 K; Standard pressure uncertainty $u(p)$: 0.06 MPa; Maximum standard liquid fraction uncertainty u(Liquid fraction percentage): 2.1%; Maximum standard relative volume uncertainty u(Relative volume): 0.035.

Table 8

Liquid fraction percentage ($100 \cdot V_{liq}/V_{tot}$) and relative volume ($V_{tot}/V_{sat}$) for the HPHT gas condensate.[a]

p	%		p	%		p	%		p	%	
MPa	V_{liq}/V_{tot}	V_{tot}/V_{sat}	/MPa	V_{liq}/V_{tot}	V_{tot}/V_{sat}	MPa	V_{liq}/V_{tot}	V_{tot}/V_{sat}	MPa	V_{liq}/V_{tot}	V_{tot}/V_{sat}
T=298.15 K			*T*=323.15 K			*T*=348.15 K			*T*=363.15 K		
73.43		0.987	71.36		0.974	65.34		0.971	65.31		0.958
73.08		0.989	70.97		0.976	65.21		0.972	64.93		0.959
72.12		0.991	70.08		0.979	64.29		0.976	63.99		0.964
71.17		0.994	69.10		0.982	63.29		0.981	62.96		0.969
70.19		0.997	68.11		0.985	62.34		0.985	61.98		0.973
70.02		0.998	67.13		0.988	61.33		0.990	60.99		0.979
69.85		0.998	66.10		0.992	60.31		0.995	59.99		0.984
69.72		0.998	65.12		0.996	60.22		0.996	59.00		0.990
69.57		0.999	64.93		0.997	60.10		0.996	57.97		0.995
68.48		1.002	64.83		0.997	60.02		0.997	57.89		0.996
67.30		1.006	64.80		0.997	59.90		0.997	57.73		0.997

64.47		1.014	64.69		0.998	59.80		0.998	57.63		0.997
61.87		1.023	63.85		1.001	59.70		0.998	57.61		0.997
59.58		1.032	63.02		1.005	59.68		0.998	57.05		1.001
57.33	0.06	1.041	60.99		1.013	59.04		1.002	56.56		1.004
55.12	0.17	1.050	58.96		1.022	58.46		1.005	55.27		1.012
53.11	0.42	1.059	57.19		1.030	56.98		1.013	54.06		1.020
51.29	0.72	1.069	55.46	0.03	1.039	55.53		1.022	52.87		1.028
44.74	1.98	1.106	53.79	0.13	1.048	54.11		1.030	51.76		1.036
39.66	3.41	1.145	52.18	0.34	1.057	52.87	0.01	1.038	50.72	0.03	1.044
35.59	4.75	1.184	50.77	0.53	1.066	51.64	0.07	1.047	49.68	0.19	1.053
32.37	5.89	1.224	45.64	1.63	1.102	50.44	0.24	1.055	48.69	0.31	1.061
28.71	7.12	1.285	41.46	2.74	1.139	49.28	0.41	1.064	45.18	1.03	1.094
25.95	8.25	1.346	38.01	3.67	1.176	45.28	1.25	1.098	42.21	1.61	1.127
20.44	9.71	1.551	35.19	4.66	1.213	41.94	2.11	1.133	39.67	2.43	1.161
15.48	9.28	1.967	31.82	5.75	1.270	39.15	2.81	1.167	37.48	2.95	1.194
			29.17	6.37	1.327	36.74	3.38	1.203	34.67	3.64	1.245
			23.44	7.92	1.520	33.73	4.42	1.256	32.35	4.26	1.296
			17.78	7.66	1.909	31.32	5.04	1.309	26.84	5.42	1.468
			13.60	6.54	2.494	25.71	6.20	1.488	20.68	5.65	1.813
			10.56	5.02	3.277	19.68	6.48	1.849	15.84	4.90	2.334
			8.31	3.79	4.256	15.05	5.51	2.394	12.25	3.92	3.030
						11.64	4.30	3.121	9.59	3.02	3.900
						9.13	3.39	4.031			
T=393.15 K			*T*=423.75 K			*T*=448.15 K			*T*=473.15 K		
60.27		0.957	59.24		0.933	54.22		0.941	54.18		0.905
59.63		0.960	56.51		0.952	53.84		0.944	51.22		0.934
58.64		0.966	55.51		0.960	52.85		0.953	50.24		0.944
57.64		0.973	54.51		0.968	51.87		0.962	49.25		0.955
56.63		0.980	53.50		0.976	50.88		0.972	48.23		0.966
55.66		0.987	52.51		0.985	49.88		0.982	47.25		0.978
54.64		0.994	51.49		0.994	48.88		0.993	46.24		0.991
54.56		0.995	51.44		0.995	48.80		0.994	46.08		0.993
54.47		0.995	51.33		0.996	48.70		0.995	46.03		0.994
54.35		0.996	51.23		0.997	48.60		0.996	45.97		0.995
54.25		0.997	51.11		0.998	48.50		0.997	45.87		0.996
54.14		0.998	51.02		0.999	48.45		0.998	45.83		0.997
54.03		0.999	50.98		0.999	48.41		0.999	45.73		0.998
53.95		1.000	50.93		1.000	48.35		0.999	45.68		0.999
53.90		1.000	50.90		1.000	48.31		1.000	45.63		0.999
53.87		1.000	50.83		1.001	48.25		1.000	45.58		1.000
53.82		1.001	50.78		1.001	48.25		1.000	45.53		1.001
53.75		1.001	50.73		1.002	48.03		1.003	45.34		1.003
53.65		1.002	50.69		1.002	47.80		1.005	45.17		1.005
53.61		1.003	50.69		1.002	47.28		1.012	44.74		1.011
53.23		1.006	50.43		1.005	46.73		1.018	44.33		1.017
52.85		1.009	50.15		1.008	46.22		1.025	43.92		1.023
51.90		1.016	49.47		1.015	45.72		1.031	43.51		1.029
51.01		1.024	48.76		1.022	45.25		1.038	43.12		1.035
50.20		1.031	48.16		1.029	44.75	0.00	1.044	42.75		1.041
49.38		1.039	47.53		1.035	44.29	0.00	1.051	42.36	0.00	1.047
48.57	0.01	1.046	46.94		1.042	42.52	0.08	1.077	40.93	0.00	1.071
47.82	0.06	1.054	46.32		1.049	40.94	0.22	1.103	39.60	0.09	1.095
47.09	0.13	1.062	45.79	0.02	1.056	39.48	0.39	1.129	38.38	0.20	1.119
44.43	0.57	1.092	43.65	0.20	1.085	38.13	0.57	1.155	37.23	0.30	1.143
42.08	1.04	1.123	41.76	0.51	1.113	36.31	0.83	1.194	35.66	0.48	1.179
40.02	1.50	1.154	40.05	0.79	1.141	34.68	1.07	1.234	34.23	0.68	1.215
38.17	1.87	1.185	38.49	1.05	1.169	30.29	1.59	1.365	30.29	1.03	1.335
35.78	2.40	1.232	36.41	1.41	1.212	24.43	2.08	1.630	24.81	1.40	1.577
33.71	2.86	1.279	34.58	1.76	1.255	19.18	2.09	2.028	19.70	1.52	1.941
28.56	3.81	1.436	29.81	2.37	1.398	15.02	1.89	2.560	15.96	1.38	2.367
22.36	4.19	1.752	23.71	2.86	1.685	11.85	1.54	3.225	13.14	1.25	2.854

17.23	3.85	2.228	18.43	2.82	2.118		
13.35	3.12	2.865	14.35	2.41	2.696		
10.47	2.47	3.661	11.28	1.90	3.420		

[a]Standard temperature uncertainty $u(T)$: 0.02 K; Standard pressure uncertainty $u(p)$: 0.06 MPa; Maximum standard liquid fraction uncertainty u(Liquid fraction percentage): 1.6%; Maximum standard relative volume uncertainty u(Relative volume): 0.063.

The experimental values of the relative volume and the liquid fraction are plotted as a function of pressure in Fig. 9 for the HPHT volatile oil and the HPHT gas condensate at selected temperatures. The model predictions are also depicted in this figure. As regards the relative volume at the selected temperatures, it is not possible to observe a clear transition from the single-phase system to the two-phase system in the relative volume curves vs. pressure due to the small contrast between gas and liquid compressibilities associated to the phase transition. Maximum relative expansions of 2.3 and 4.3 were measured for the HPHT volatile oil and the HPHT gas condensate, respectively. A good prediction of this property was found through the models studied in this work.

As regards the liquid fraction of the HPHT volatile oil in Fig. 9 (b), the experimental data show the typical liquid fraction behaviour under expansion corresponding to a bubble point, i.e. a liquid fraction of 100% is observed at the saturation pressure, and the value of this property decreases with a further decrease in the pressure below the bubble point. The best liquid fraction predictions for the HPHT volatile oil are obtained with the cubic EoSs, whereas PC-SAFT can reproduce in general the slope of liquid fraction decrease with pressure and the deviations in the prediction are mainly caused by the poor prediction of the saturation pressure of the HPHT volatile oil through this EoS. Finally, concerning the liquid fraction of the HPHT gas condensate, it can be observed in Fig. 9 (d) that the experimental data correspond to the typical behaviour of a retrograde gas starting with a liquid fraction of 0% at the saturation pressure which increases with the pressure decrease and passes through a maximum, after which the liquid fraction decreases with a further pressure decrease. An interesting feature from the experimental liquid fraction values is that negligible amount of condensate happened under

a considerable pressure decrease below the dew point, i.e. a big pressure decrease was needed in order to obtain a measurable amount of condensate, this phenomena led to a tail in the liquid fraction vs. pressure curves. The different EoSs present difficulties capturing this tail-like behaviour, as previously stated by Whitson et al. [5]. This tail becomes longer when the temperature decreases, for instance at 298.15 K, the measured dew point was 69.55 MPa, but the pressure needed to be decreased down to 57.33 MPa in order to get a measurable amount of condensate. This tail-like behaviour of the liquid drop-out was previously reported by Robinson [32], who reported a pressure decrease of 15.8 MPa below the dew point to get a 0.5% of liquid fraction for a gas condensate at 283.15 K. However, Ahmed [33] reported that the small build-up of condensate has previously been attributed to sample contamination by hydraulic fluids from various sources during drilling, production and sampling, even though he states that it could also be a feature of real reservoir fluids [33]. Our compositional analysis of the gas condensate (Table 1) does not show any obvious sample contamination. The experimental liquid fraction increases when temperature decreases due to a higher drop out of the heavier compounds at lower temperatures. A maximum liquid fraction of 9.7 % was found at 298.15 K, this value is over predicted by the models used in this work, it can be observed in Fig. 9 (d) that the model prediction for the liquid fraction of the gas condensate becomes poorer when the temperature decreases. Barnum et al. [34] gathered data for gas condensates from 17 fields, concluding that the condensation of the liquid hydrocarbons can affect the gas productivity to great extent in low productivity reservoirs. Also, Afidick et al. [35] studied near wellbore condensate accumulation in a gas condensate from the Arun field (Indonesia), this gas condensate was a lean-gas with a maximum liquid drop-out of 1.1% and they found that despite of being a lean-gas, some of the well productivities were reduced by 50%. These studies [34, 35] indicate that the amount of retrograde condensate of the HPHT gas condensate studied in the present work could affect productivity of this reservoir fluid.

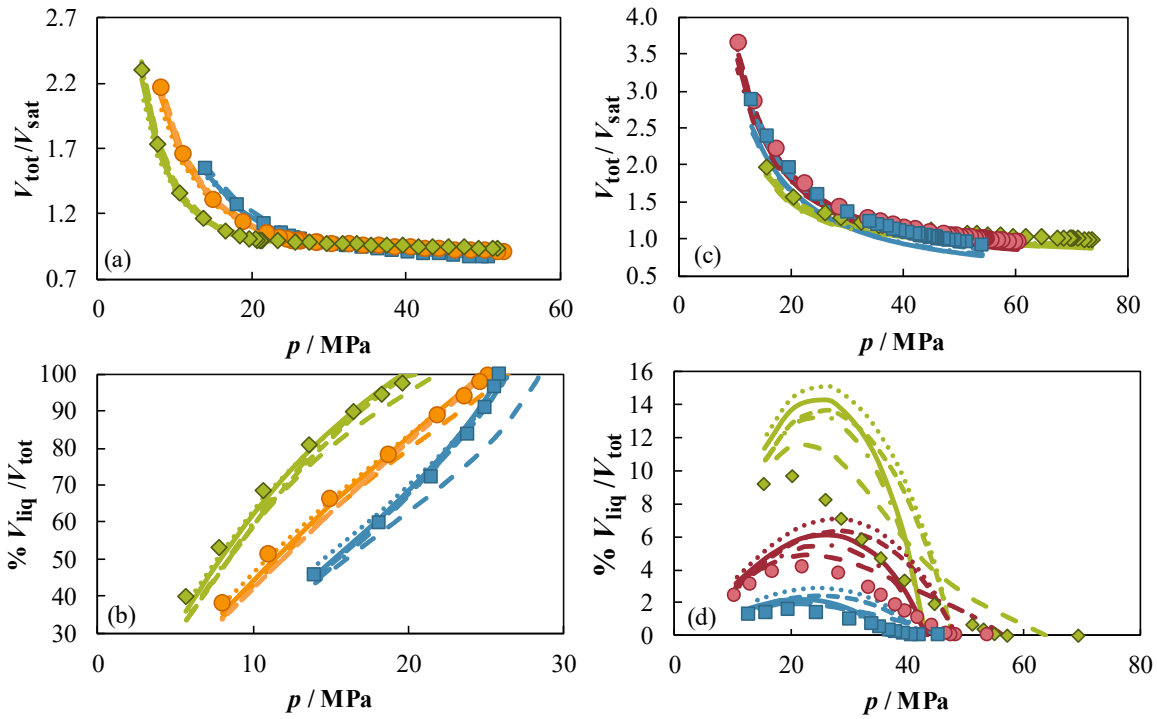

Fig. 9. Relative volume (V_{tot}/V_{sat}) and liquid fraction percentage ($100 \cdot V_{liq}/V_{tot}$) of the HPHT volatile oil (a, b) and the HPHT gas condensate (c, d) at 298.15 K (◆), 373.15 K (●), 393.15 K (●) and 473.15 K (■). Lines represent the model predictions SRK (•••), SRK-VT (– – –), PR (—), PR-VT (– • –) and PC-SAFT (— —).

A quantitative representation of the models performance for both the prediction of the relative volume and the liquid fraction percentage is given in Figs. 10 and 11, respectively. In Fig. 10 it can be observed that the relative volume predictions are generally good. For the HPHT volatile oil predictions are especially good through PR, whereas for the HPHT gas condensate the best predictions were obtained with PC-SAFT, closely followed by SRK. For the cubic EoSs the volume translation had negligible effect in the calculation of this property. In Fig. 11 it can be observed how the prediction of the liquid fraction percentage of the HPHT volatile oil is better through the cubic EoSs, as concerns the gas condensate the best prediction is obtained with PC-SAFT.

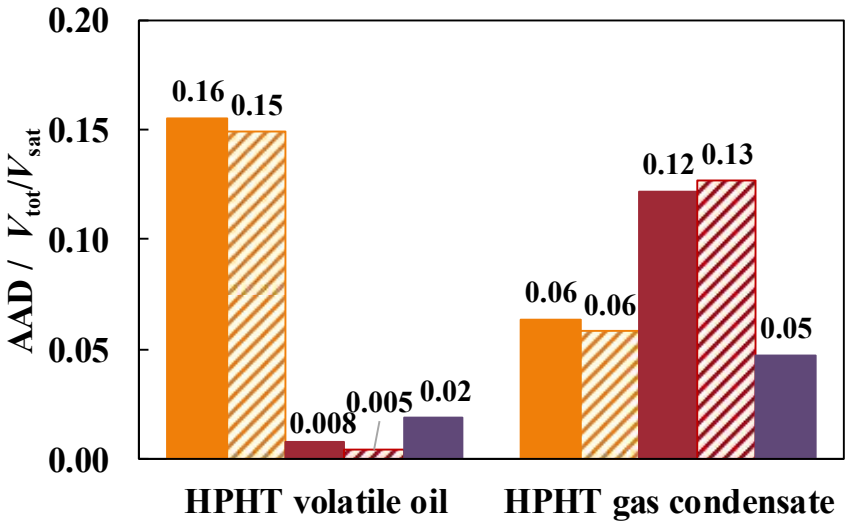

Fig. 10. Absolute average deviation for the prediction of the relative volume (V_{tot}/V_{sat}) of the HPHT reservoir fluids through SRK (solid orange), SRK-VT (striped orange), PR (solid red), PR-VT (striped red) and PC-SAFT (solid purple).

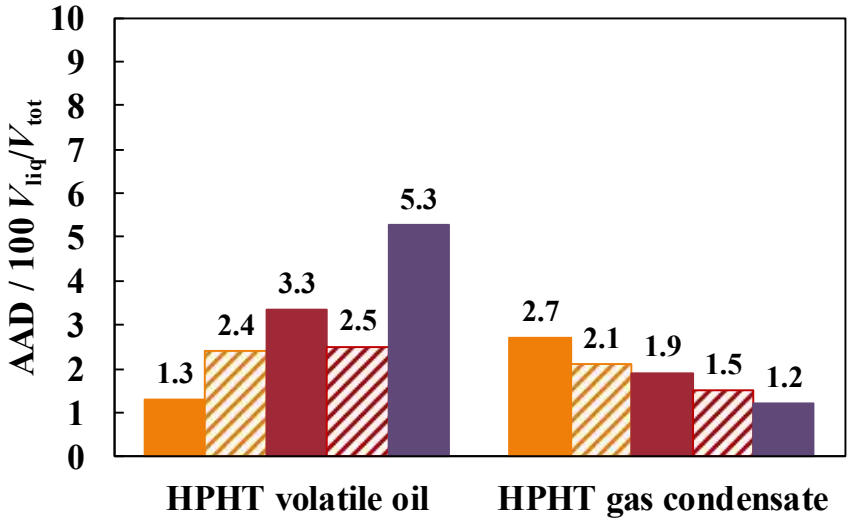

Fig. 11. Absolute average deviation for the prediction of the liquid fraction percentage ($100 \cdot V_{liq}/V_{tot}$) of the HPHT reservoir fluids through SRK (solid orange), SRK-VT (striped orange), PR (solid red), PR-VT (striped red) and PC-SAFT (solid purple).

Finally, the overall deviations for various properties of the two HPHT reservoir fluids calculated by the five models are summarized in Table 9. The smallest deviations and those "sufficiently" close to the smallest deviations are marked in bold letters. The definition of "sufficiently" close is a bit arbitrary. For density, compressibility and saturation pressure, we select values differing from the smallest value by less than 0.5. For relative volume and liquid

fraction, we marked essentially just the smallest deviations. Note that the deviations for density, compressibility and saturation pressures are relative and those for relative volume and liquid fraction are absolute. The table provides an overview of the performance of the five models. It is again difficult to single out a model that performs always the best for the studied properties although PC-SAFT tends to give smaller deviations as indicated by the number of bold letters. Among these properties, the performance of saturation pressure prediction is case-dependent and it is difficult to make a general conclusion which model is better. This is somewhat in agreement with our previous observations [3, 7, 9, 22]. For reservoir fluids, the prediction is also affected by the characterization procedure and uncertainties in interaction parameters and other characterized model parameters. It is therefore more difficult to expect that a model is consistently much better than others in the saturation pressure calculation. It should be noted that the deviations in liquid fraction are closely related to the deviations in saturation pressure. Although the vapor- and liquid-phase densities are also used in the calculation of liquid fractions, the correct location of the saturation pressure is apparently the most influencing factor. Our comparison here is for predictive calculation. For models tuned against saturation pressure, the effect of density modeling may become more visible. The calculation of relative volumes is generally insensitive to the models partly because the two-phase total volume is controlled mainly by the vapor phase. The single-phase density and compressibility are related to the volumetric performance of EoS models. Volume translation is obviously needed to improve the density calculation for SRK and PR. But the effect of volume translation on compressibility is not as straightforward. PR-VT, SRK-VT and PC-SAFT performs almost equally well for the volumetric properties with PC-SAFT seemingly slightly better in compressibility. It should be noted that PR-VT and SRK-VT have used the experimental density of C_7^+ through characterization.

It would be useful if the performance of an EoS can be linked to the methane content. The methane mole fraction for the volatile oil is around 49% and that for the gas condensate is around 83%. The density prediction improves a lot for SRK, deteriorates clearly for PR, and deteriorates slightly for PC-SAFT. The changes for SRK and PR can be explained by the fact that SRK describes methane gas density better than PR. But the performance change in compressibility is more difficult to explain, and so are the changes for the volume translated versions of SRK and PR. Regarding the saturation pressure, the prediction worsens for SRK and PR and improves for PC-SAFT when the methane fraction increases. However, we note that the above observations cannot be generalized even for the densities from SRK and PR. In our previous studies for well-defined mixtures containing methane [7-9], the trends with the methane content are not always in agreement with the observations in this study. For instance, although the density prediction by SRK improves with the methane content for two seven-component synthetic mixtures [8], the prediction by PR also improves with the methane content.

One consideration to involve PC-SAFT in the comparison is to see whether this advanced EoS shows some particular advantages over classical cubic models in describing some challenging reservoir fluids systems. PC-SAFT is apparently more complex than SRK and PR. But its robustness is comparable to SRK and PR in practical phase equilibrium calculations. This is especially the case if the Wertheim association term is not used, as in this study for hydrocarbon systems. The potential advantage for PC-SAFT without the association term comes from its more rigorous repulsive and attractive terms. Our previous comparative study [22] has shown that PC-SAFT is clearly better than cubics in describing volumetric properties for pure components but similar to cubics in binary and multicomponent VLE calculations. After C_7^+ characterization [3, 22], the advantage of using PC-SAFT in PVT calculation becomes less clear. This can be attributed to many reasons, such as the uncertainty associated with the C_7^+

characterization, the sensitivity of the model parameters, the quality of the PVT data, and the type of fluids used in comparison. Regarding the sensitivity, our previous study [22] shows that PC-SAFT is more sensitive to its model parameters. This can make PC-SAFT more susceptible to uncertainties in reservoir fluids. In practice, tuning of a PVT model is usually performed to anchor the model to some experimental data, which can somehow reduce the influence from the uncertainties. For further application of PC-SAFT in reservoir fluids modelling, one major challenge is to identify situations where PC-SAFT can clearly outperform the classical models. Answering the challenge calls for both theoretical analyses indicating where PC-SAFT can be more advantageous and more experimental data for challenging systems like HPHT fluids to test the hypotheses.

Table 9
Summary of the overall deviations for different properties of the two HPHT reservoir fluids.

	SRK	SRK-VT	PR	PR-VT	PC-SAFT
	Volatile Oil				
Single-phase density	14	**1.1**	4.5	**1.3**	**1.3**
Single-phase compressibility	10.8	11.3	11.5	10.3	**9.7**
Saturation pressure	**1.6**	—	2.2	—	6.1
Relative volume	0.16	0.15	0.008	**0.005**	0.02
Liquid fraction	**1.3**	2.4	3.3	2.5	5.3
	Gas condensate				
Single-phase density	2.7	2.4	6.5	**0.6**	2.0
Single-phase compressibility	5.6	8.6	7.6	5.7	**4.4**
Saturation pressure	14	—	23	—	**3.5**
Relative volume	0.06	0.06	0.12	0.13	**0.05**
Liquid fraction	2.7	2.1	1.9	1.5	**1.2**

4. Conclusions

As a continuation of our previous studies on HPHT fluids, we extend our measurement to real reservoir fluids including one HPHT volatile oil and one HPHT gas condensate. We systematically measured the single-phase density, single-phase compressibility, saturation pressure, and liquid fraction in the two-phase region of these two fluids. The measurement was carried out in a wide temperature and pressure range, with maximum temperature and pressure

reaching 473.15 K and 140 MPa, respectively. Since it is difficult to mimic completely the phase behavior of real reservoir fluids with well-defined synthetic mixtures, the measured data is valuable for developing and evaluating relevant models for HPHT applications.

We also compared experimental results with model predictions by common cubic EoSs (SRK and PR), their volume translated versions (SRK-VT and PR-VT), and the more advanced PC-SAFT model. The saturation pressure calculation is case-dependent: the simple SRK and PR models perform better than PC-SAFT for the volatile oil whereas PC-SAFT performs better for the gas condensate. It is difficult to generalize this to other fluids. The HPHT gas condensate shows a minute amount of liquid drop-out in a considerable pressure range below the dew point. None of the current models can capture this long tail-like liquid drop-out curve. For volumetric properties like density and compressibility, PC-SAFT is clearly better than SRK and PR especially in density but PC-SAFT, PR-VT and SRK-VT perform similarly in density calculation for the two fluids investigated here. PC-SAFT seems to be slightly better in compressibility prediction but the difference is not large. Overall, the findings from the model comparison in this study are in certain agreement with the findings from our previous studies [7-9]. One can generally expect that SRK, PR and PC-SAFT perform similarly in equilibrium calculation whereas PC-SAFT may be slightly better in volumetric properties. However, the difference between models seems to be blurred for ill-defined reservoir fluids. The performance of models can well vary with the fluid type. The two fluids investigated here have relatively light C_7^+ and their overall compositions fall into the range of reservoir fluids with medium gas oil ratios. It is recommended to study experimentally and through modeling other types of HPHT reservoir fluids, e.g., heavier oil systems or even lighter gas systems, in order to give a more complete picture of the performance of various models in modeling HPHT reservoir fluids.

Acknowledgements
This work has been carried out under the NextOil project sponsored by the Innovation Fund Denmark, DONG E&P and Maersk Oil (Jr. nr. 113-2012-1).

References

[1] A. Shadravan, M. Amani, HPHT 101: What every engineer or geoscientist should know about high pressure high temperature wells, in: SPE Kuwait International Petroleum Conference and Exhibition, Society of Petroleum Engineers, Kuwait City, Kuwait, 2012. https://doi.org/10.2118/163376-MS.
[2] H. Alboudwarej, J.M. Sheffield, M. Srivastava, S.S. Wu, L. Zuo, A. Inouye, D. Zhou, A. Oghena, High pressure gas EOR PVT experimental programs: challenges in measurements and data interpretations, in: SPE Improved Oil Recovery Conference, Society of Petroleum Engineers, Tulsa, Oklahoma, USA, 2018. https://doi.org/10.2118/190257-MS.
[3] F. Varzandeh, E.H. Stenby, W. Yan, General approach to characterizing reservoir fluids for EoS models using a large PVT database, Fluid Phase Equilib., 433 (2017) 97-111. https://doi.org/10.1016/j.fluid.2016.10.018.
[4] C. Shi, R.N. Horne, K. Li, Optimizing the productivity of gas/condensate wells, in: SPE Annual Technical Conference and Exhibition, Society of Petroleum Engineers, San Antonio, Texas, USA, 2006. https://doi.org/10.2118/103255-MS.
[5] C.H. Whitson, Ø. Fevang, T. Yang, Gas Condensate PVT: What's Really Important and Why?, in: IBC Conference on Optimization of Gas Condensate Fields, London, 1999.
[6] A. Najafi-Marghmaleki, A. Tatar, A. Barati-Harooni, M. Arabloo, S. Rafiee-Taghanaki, A.H. Mohammadi, Reliable modeling of constant volume depletion (CVD) behaviors in gas condensate reservoirs, Fuel, 231 (2018) 146-156. https://doi.org/10.1016/j.fuel.2018.04.130.
[7] T. Regueira, G. Pantelide, W. Yan, E.H. Stenby, Density and phase equilibrium of the binary system methane + n-decane under high temperatures and pressures, Fluid Phase Equilib., 428 (2016) 48-61. https://doi.org/10.1016/j.fluid.2016.08.004.
[8] T. Regueira, M.-L. Glykioti, E.H. Stenby, W. Yan, Density and compressibility of multicomponent n-alkane mixtures up to 463 K and 140 MPa, J. Chem. Eng. Data, 63 (2018) 1072-1080. https://doi.org/10.1021/acs.jced.7b00803.
[9] T. Regueira, Y. Liu, A.A. Wibowo, M. Ashrafi, F. Varzandeh, G. Pantelide, E.H. Stenby, W. Yan, High pressure phase equilibrium of ternary and multicomponent alkane mixtures in the temperature range from (283 to 473) K, Fluid Phase Equilib., 449 (2017) 186-196. https://doi.org/10.1016/j.fluid.2017.06.021.
[10] G. Soave, Equilibrium constants from a modified Redlich-Kwong equation of state, Chem. Eng. Sci., 27 (1972) 1197-1203. http://dx.doi.org/10.1016/0009-2509(72)80096-4.
[11] D.-Y. Peng, D.B. Robinson, A new two-constant Equation of State, Ind. Eng. Chem. Fundam., 15 (1976) 59-64. http://dx.doi.org/10.1021/i160057a011.
[12] G.S. Soave, An effective modification of the Benedict–Webb–Rubin equation of state, Fluid Phase Equilib., 164 (1999) 157-172. http://dx.doi.org/10.1016/S0378-3812(99)00252-6.
[13] N. von Solms, M.L. Michelsen, G.M. Kontogeorgis, Computational and physical performance of a modified PC-SAFT equation of state for highly asymmetric and associating mixtures, Ind. Eng. Chem. Res., 42 (2003) 1098-1105. https://doi.org/10.1021/ie020753p.
[14] D.L. Katz, A. Firoozabadi, Predicting phase behavior of condensate/crude-oil systems using methane interaction coefficients, SPE-6721-PA, 30 (1978) 1649-1655. https://doi.org/10.2118/6721-PA.

[15] M.J.P. Comuñas, J.-P. Bazile, A. Baylaucq, C. Boned, Density of diethyl adipate using a new vibrating tube densimeter from (293.15 to 403.15) K and up to 140 MPa. Calibration and measurements, J. Chem. Eng. Data, 53 (2008) 986-994. http://dx.doi.org/10.1021/je700737c.
[16] B. Lagourette, C. Boned, H. Saint-Guirons, P. Xans, H. Zhou, Densimeter calibration method versus temperature and pressure, Meas. Sci. Technol., 3 (1992) 699-703. https://doi.org/10.1088/0957-0233/3/8/002.
[17] J.J. Segovia, O. Fandiño, E.R. López, L. Lugo, M. Carmen Martín, J. Fernández, Automated densimetric system: Measurements and uncertainties for compressed fluids, J. Chem. Thermodyn., 41 (2009) 632-638. http://dx.doi.org/10.1016/j.jct.2008.12.020.
[18] J. Gross, G. Sadowski, Perturbed-Chain SAFT: An equation of state based on a perturbation theory for chain molecules, Ind. Eng. Chem. Res., 40 (2001) 1244-1260. http://dx.doi.org/10.1021/ie0003887.
[19] A. Péneloux, E. Rauzy, R. Fréze, A consistent correction for Redlich-Kwong-Soave volumes, Fluid Phase Equilib., 8 (1982) 7-23. https://doi.org/10.1016/0378-3812(82)80002-2.
[20] K.S. Pedersen, P.L. Christensen, Phase Behavior of Petroleum Reservoir Fluids, Taylor & Francis Group, New York, 2007.
[21] T. Yamada, R.D. Gunn, Saturated liquid molar volumes. Rackett equation, J. Chem. Eng. Data, 18 (1973) 234-236. https://doi.org/10.1021/je60057a006.
[22] W. Yan, F. Varzandeh, E.H. Stenby, PVT modeling of reservoir fluids using PC-SAFT EoS and Soave-BWR EoS, Fluid Phase Equilib., 386 (2015) 96-124. https://doi.org/10.1016/j.fluid.2014.11.022.
[23] K.S. Pedersen, P. Thomassen, A. Fredenslund, Characterization of gas condensate mixtures, Taylor & Francis, New York, 1989.
[24] K.S. Pedersen, A. Fredenslund, P. Thomassen, Properties of oils and natural gases, Gulf Publishing Inc, Houston, 1989.
[25] C.H. Twu, An internally consistent correlation for predicting the critical properties and molecular weights of petroleum and coal-tar liquids, Fluid Phase Equilib., 16 (1984) 137-150. https://doi.org/10.1016/0378-3812(84)85027-X.
[26] B.I. Lee, M.G. Kesler, A generalized thermodynamic correlation based on three-parameter corresponding states, AIChE J., 21 (1975) 510-527. https://doi.org/10.1002/aic.690210313.
[27] S. Skjold-Jørgensen, Gas solubility calculations. II. Application of a new group-contribution equation of state, Fluid Phase Equilib., 16 (1984) 317-351. https://doi.org/10.1016/0378-3812(84)80005-9.
[28] G.M. Kontogeorgis, E.C. Voutsas, I.V. Yakoumis, D.P. Tassios, An Equation of State for associating fluids, Ind. Eng. Chem. Res., 35 (1996) 4310-4318. https://doi.org/10.1021/ie9600203.
[29] W. Yan, G.M. Kontogeorgis, E.H. Stenby, Application of the CPA equation of state to reservoir fluids in presence of water and polar chemicals, Fluid Phase Equilib., 276 (2009) 75-85. https://doi.org/10.1016/j.fluid.2008.10.007.
[30] W.A. Burgess, B.A. Bamgbade, I.K. Gamwo, Experimental and predictive PC-SAFT modeling results for density and isothermal compressibility for two crude oil samples at elevated temperatures and pressures, Fuel, 218 (2018) 385-395. https://doi.org/10.1016/j.fuel.2017.12.101.
[31] P. Ungerer, B. Faissat, C. Leibovici, H. Zhou, E. Behar, G. Moracchini, J.P. Courcy, High pressure-high temperature reservoir fluids: investigation of synthetic condensate gases containing a solid hydrocarbon, Fluid Phase Equilib., 111 (1995) 287-311. https://doi.org/10.1016/0378-3812(95)02771-6.
[32] D.B. Robinson, The interface between theory and experiment, Fluid Phase Equilib., 52 (1989) 1-14. https://doi.org/10.1016/0378-3812(89)80306-1.

[33] T. Ahmed, Chapter 4 - PVT properties of crude oils, in: T. Ahmed (Ed.) Equations of State and PVT Analysis (Second Edition), Gulf Professional Publishing, Boston, 2016, pp. 239-466.
[34] R.S. Barnum, F.P. Brinkman, T.W. Richardson, A.G. Spillette, Gas condensate reservoir behaviour: Productivity and recovery reduction due to condensation, in: SPE Annual Technical Conference and Exhibition, Society of Petroleum Engineers, Dallas, Texas, 1995. https://doi.org/10.2118/30767-MS.
[35] D. Afidick, N.J. Kaczorowski, S. Bette, Production performance of a retrograde gas reservoir: A case study of the Arun Ffield, in: SPE Asia Pacific Oil and Gas Conference, Society of Petroleum Engineers, Melbourne, Australia, 1994. https://doi.org/10.2118/28749-MS.